Hindawi
Advances in Civil Engineering
Volume 2021, Article ID 6616546, 11 pages
https://doi.org/10.1155/2021/6616546

Research Article

Research on Permeability Coefficient of Heterogeneous Geomaterials Based on Digital Images

Bowen Liu,[1] **Junbin Chen**,[2] **and Xinpin Ding**[3]

[1]*School of Energy and Mining Engineering, China University of Mining and Technology (Beijing), Beijing 100083, China*
[2]*Hulunbuir Dongming Mining Co., Ltd., Hulunbuir 021500, Inner Mongolia, China*
[3]*China Coal Research Institute, Beijing 100013, China*

Correspondence should be addressed to Bowen Liu; bqt1800101016@student.cumtb.edu.cn

Received 28 November 2020; Revised 29 December 2020; Accepted 25 January 2021; Published 23 February 2021

Academic Editor: Sang-Bing Tsai

According to the relationship between permeability and porosity of geotechnical materials, a finite element model representing pore and solid particles is generated randomly according to the porosity of a given finite element calculation model. According to Darcy's law of flow distribution and steady seepage in the finite element random simulation section, the equivalent permeability coefficients at different porosities are calculated, and the relationship between the equivalent permeability coefficient and the porosity of rock and soil is studied. The results show that the equivalent permeability coefficient is proportional to the porosity with the same pore size. In order to study the seepage characteristics of structural planes of nonmaterial geotechnical materials in different strata contact zones, the formulas for calculating the deformation parameters and permeability coefficients of heterogeneous rock masses with single nonmaterial geotechnical materials are deduced theoretically, and the correctness and applicability of the formulas are verified by experiments. The rock mass sample selected in this paper is granite, which is simulated and analyzed by sandstone in the experiment. The results show that the permeability coefficients of coarse sandstone, fine sandstone, and heterogeneous rock mass are different under the same water pressure and confining pressure. This shows that the lithology on both sides of the nonmaterial geotechnical material surface has a significant influence on the permeability of the nonmaterial geotechnical material rock mass; the permeability coefficient of the nonmaterial geotechnical material rock mass decreases with the increase of confining pressure, the numerical change is limited to a certain confining pressure range, and the permeability coefficient tends to be stable when the confining pressure reaches a certain value. Comparing the theoretical calculation value of permeability coefficient of rock mass with the experimental result, it is found that the two values are in good agreement, which indicates the correctness and applicability of the theoretical calculation formula of permeability coefficient of rock mass of single intangible geotechnical material.

1. Introduction

The nonmaterial geotechnical materials of natural rock mass have some problems, such as uneven surface, undulating surface, different penetration rate, and coincidence degree of nonmaterial geotechnical materials [1]. The roughness of the surface, the filling material state, and the surrounding stress will change the gap width of the nonmaterial geotechnical materials [2–5]. In engineering practice, in order to avoid excessive errors caused by using cubic law to solve seepage problems, many scholars have corrected the cubic law appropriately [6]. Tsang extended the gap width distribution function to the two-dimensional nonmaterial geotechnical material surface and thought that the gap width conformed to lognormal distribution and could draw equivalent nonmaterial geotechnical material [7–12] by computer simulation. Brown obtained the gap width variation coefficient C_v through seepage test and analysis. Neuzil assumes that the width of the gap varies along the vertical flow and obtains the distribution function of the width of the gap [13, 14]; Lee establishes the correlation formula between the roughness coefficient and the fractal dimension; Scesi carries out experimental studies on seepage characteristics of different JRC artificial nonmaterial geotechnical materials [15–17].

However, when the Reynolds number is too large, it will lead to turbulence in immaterial geotechnical materials. Chen, Meheust, Lomize, Wang Yuan, and Subaoyu and other scholars at home and abroad have proposed turbulence calculation formulas, but the Darcy formula is still used for most seepage problems. On the study of shear strength of ionic curing agent modified clay, it is mainly considered that ionic curing agent can improve the mechanical properties of clay [18–21], in which cohesion c value increases significantly, while internal friction angle φ value increases slightly. Therefore, it is proposed that ionic curing agent mainly affects shear properties by influencing cohesion. However, the sensitivity of shear strength to C and φ has not been considered in this kind of research. For example, in the construction of water conservancy and hydropower projects, the slight change of φ value has a significant impact on the project cost. Therefore, the mechanism of soil modification by the ionic solidifying agent cannot be simply judged by the change of value [22]. On the other hand, it is necessary to exclude the influence of φ value and to study the mechanical properties of ionic curing agent modified clay by tensile test [23]. Many scholars at home and abroad have proved that when the Reynolds number is less than 2300 in the laminar flow range of immaterial geotechnical materials, the seepage of immaterial geotechnical materials satisfies the cubic law.

In recent years, it is necessary to fully consider the situation of intangible geotechnical materials in tunnel surrounding rocks. In particular, in the construction of tunnels in high water pressure and water-rich areas, many problems of permeability stability of rock mass have arisen [24]. The problem of permeability stability of intangible geotechnical materials has seriously affected the safety of practical projects. Therefore, it is more and more important to study the permeability characteristics of the rock mass. To ensure the safety of tunnel engineering in high water pressure and rich water area, it is necessary to grasp the physical and mechanical properties and seepage properties of nonmaterial geotechnical materials in high water pressure and rich water area. At present, many geotechnicians at home and abroad have made good achievements in the permeability characteristics of monoimmaterial geotechnical materials, but little research has been done on the permeability characteristics and mechanical properties of cross-immaterial geotechnical materials and filling immaterial geotechnical materials [25–28]. Therefore, it is an urgent problem to study the permeability and hydraulics of vertically intersecting nonmaterial geotechnical materials and filling nonmaterial geotechnical materials under different conditions of surrounding rock (lateral pressure), axial pressure, water pressure, and area of nonmaterial geotechnical materials. Nonmaterial geotechnical materials are heterogeneous and discontinuous granular materials consisting of larger boulders and fine-grained soils. It is difficult to reveal the complex deformation and failure mechanism of nonmaterial geotechnical materials by experimental research and traditional mechanical analysis methods of continuous media. The particle discrete element method (PDE) can simulate the nonlinearity, large deformation, and complex interaction of particles, so it is more suitable to study the mechanical properties and deformation failure mechanism of nonmaterial geotechnical materials at the mesoscopic level. Choo et al. [29, 30], based on the three-dimensional particle discrete element method, carried out a numerical simulation of large-scale direct shear tests of nonmaterial geotechnical materials with different rock content and lithology, but there are some differences between the simplified sphere and the actual situation in the model. Asadi and Ataie-Ashtiani [31] carried out two-dimensional particle flow numerical simulation of biaxial test and direct shear test on the measured model of immaterial geotechnical materials obtained from digital image processing and compared the mechanical properties and deformation failure characteristics of immaterial geotechnical materials and homogeneous soil. Mao et al. [32–35] used two-dimensional particle flow to simulate the biaxial test and direct shear test of nonmaterial geotechnical materials and analyzed the influence of stone content, shape, and roughness of blocks on the internal friction angle and cohesion of nonmaterial geotechnical materials. However, the regular two-dimensional and multidimensional polygons with triangular and rectangular shapes of blocks in the model are still different from the three-dimensional irregular shapes of blocks in nature. Hamoudi et al. [36–39] proposed a random generation technology of irregular block rock three-dimensional discrete element model and established a three-dimensional discrete element model of nonmaterial geotechnical materials in accordance with macrostatistical law. The large triaxial test of nonmaterial geotechnical materials was simulated numerically, and the deformation and failure mechanism of nonmaterial geotechnical materials was analyzed in depth.

It can be seen from the existing research results that although there have been many research results on the permeability coefficient of nonmaterial geotechnical materials, none of them has systematically explored the influence of the micromechanical parameters of nonmaterial geotechnical materials on their macromechanical response. This is precisely the key problem to be solved in the study of mechanical properties of geotechnical materials using digital images. Therefore, based on the permeability coefficient of nonmaterial geotechnical materials proposed in this paper, the digital image processing flow of nonmaterial geotechnical materials is carried out, and the ratios of normal stiffness of different rock-soil particles, normal tangential stiffness ratio of different rock-soil particles, and friction coefficient of different rock-soil particles are obtained. The stress-strain characteristics of nonmaterial geotechnical materials under different bond strengths between rock and soil particles are analyzed. The micromechanism of the influence of different micromechanical parameters of particles on macromechanical properties is analyzed from the aspects of microcrack evolution, friction work, and average rotation of rock particles. Then, based on the Fracture-Rock displacement model under three-dimensional stress, the formula for calculating the permeability coefficient of nonmaterial geotechnical materials is derived [40]. Finally, the correctness and applicability of the new formula for

calculating the permeability coefficient of nonmaterial geotechnical materials are verified by experiments.

2. Proposed Method

2.1. Basic Principles of Digital Image. The digital speckle method is usually used in the correlation processing of surface deformation of two measured objects. The basic principle is to select a point in the image and take the small area centered on the point as the sample subset. A subset matching the sample subset is found in the deformable speckle image. Then, by comparing and analyzing the position difference of the two subsets, the deformation of the point can be obtained. In this process, the digital image is transformed into a gray-scale image to obtain the deformation of the surface of the object under test [41]. It can be said that the speckles on the surface of the object under test and the corresponding gray-scale image are the bearing tools of deformation information.

The function of the initial digital image (initial subset) is expressed as

$$F_1 = \{f_1(x, y)\, x = 1, 2, \ldots, N_1; y = 1, 2, \ldots, N_2\}. \quad (1)$$

The deformed digital image (deformed subset) function is expressed as

$$F_2 = \{f_2(x, y)\, x = 1, 2, \ldots, N_1; y = 1, 2, \ldots, N_2\}. \quad (2)$$

The gray distribution functions are $f_1(x, y)$ and $f_2(x, y)$ of the two digital images before and after surface deformation, and the size of N_1 and N_2 images, respectively, is used in the formula. The initial position of a point on the surface of the measured object is (x, y) and the displacement field function is assumed. Geotechnical material images obtained by various image acquisition devices contain abundant internal structure information of geotechnical materials in their gray value and color. With the help of image processing technology, the digital image of geotechnical materials can be analyzed quantitatively, and the microstructural characteristics such as shape, content, size, and orientation of blocks in geotechnical bodies can be analyzed. The extraction of interior structural features of nonmaterial geotechnical materials can use image processing to obtain digital images of nonmaterial geotechnical materials through digital photography and then identify the shape of blocks by image processing technology. The stochastic database of rock shape is established through a large number of data acquisition so that the stochastic model of nonmaterial geotechnical material structure can be acquired subsequently.

The digital image acquisition system is mainly composed of three parts: camera, light source, and computer image analysis system [42]. The two-dimensional shape image of block stone is acquired by the camera and then imported into the computer system for particle shape recognition. Repeat this operation to obtain a large number of different shapes of block stones, and establish a stochastic database of block stones.

Because of the influence of external environment factors (such as illumination, instrument, and color difference of minerals in rock), the image acquired by image acquisition machine usually has a lot of image noise, which makes it difficult to be directly used in digital image processing and analysis. Therefore, the existing image processing software (such as Photoshop) must be used to preprocess the original image, reduce or eliminate the influence of adverse factors, and extract the object needed to study (as shown in Figure 1), so as to facilitate the next step to use image segmentation algorithm to identify the shape of the block boundary.

After preprocessing, the gray value of the boundary of the block stones has a sudden change. Canny edge detection algorithm can be used to extract the pixels of the edge points, and all the coordinates of the block stones edge can be obtained [43]. At present, the most commonly used method of edge detection is to detect the discontinuity of image brightness or gray value. The discontinuity can be detected by the first or second derivative of its function, which is usually expressed by a gradient.

The basic property of the gradient vector is that it points to the direction of the maximum change rate of f at (x, y). The angle of maximum change rate is

$$\alpha(x, y) = \arctan\left(\frac{G_y}{G_x}\right). \quad (3)$$

The methods are summarized as follows. (1) *Noise Removal*. A Gaussian filter with a specified standard deviation is used to smooth the image and reduce the influence of noise [44]. (2) Calculate the image edge gradient. The local gradient $g(x, y)$ and the edge direction $\alpha(x, y)$ at each point are calculated. The edge point is defined as the point with the greatest local strength in the gradient direction. (3) *Nonmaximum Gradient Suppression*. The edge points determined by Article 1 will lead to ridges in the gradient magnitude image. The algorithm tracks the top of all ridges and sets all the pixels that are not at the top of the ridge to zero so as to output a given fine line, i.e., nonmaximum suppression processing. Pixels are processed by two thresholds, $T_1 < T_2$. Pixels whose values are greater than T_2 are called strong edge pixels, and those between T_1 and T_2 become weak edge pixels. (4) *Produce the Edge*. The algorithm integrates weak pixels into strong pixels and performs edge links.

2.2. Anisotropy of Geotechnical Materials. The difference between mechanical parameters, structural characteristics, and the stress-strain relationship of engineering materials in different directions is called anisotropy. It is one of the important physical and mechanical properties of soil and has a great influence on the properties of soil. Generally speaking, anisotropy can be divided into primary anisotropy and secondary anisotropy or stress-induced anisotropy according to the causes and manifestations of anisotropy. Primary anisotropy refers to the difference of mechanical properties and parameters in different directions of natural soil or artificial soil in the process of sedimentation or filling due to various reasons. This is related to the secondary anisotropy of soil particles in the course of sediment,

Figure 1: Preprocessing of a stone image.

especially in the complex loading state. The change of stress state results in the change of mechanical properties and parameters caused by loading in different directions. For example, the natural consolidation state of soil is a K_0 consolidation state rather than an isobaric state, and anisotropy will occur after consolidation. The change of external load may also lead to the rearrangement of particles, thus changing the anisotropy of soil.

The stress-strain relationship of geotechnical materials is influenced by stress history and stress state and has a strong correlation with stress path. The anisotropy of soil is mainly manifested in the fact that the undisturbed soil is always formed under certain stress historical conditions, and the soil particle structure produces directional arrangement, forming a certain degree of primary anisotropy macroscopically. With the application of external loads, the soil in a working state passes through a certain stress path and reaches a certain stress state. In this process, the particle structure of the upper body changes again and shows different stress-denaturation characteristics in different stress directions. Relative to the primary anisotropy, it is called secondary anisotropy. The effects of stress history, stress path, and stress state on the stress-strain relationship of soils are mainly embodied in the formation process of anisotropy. In a sense, soil, as a frictional and granular discontinuous medium material, is an engineering material with both primary anisotropy and secondary anisotropy. For soil with primary anisotropy, the macroscopic behavior is different in strength and deformation law in different directions. Therefore, many researchers cut specimens from undisturbed soils at different dips in the direction of deposition and then conduct direct shear or conventional triaxial tests to determine the degree of anisotropy. There are many research results in this area, and there are relatively consistent conclusions.

The study of primary anisotropy is mainly focused on strength, which can reflect the correct selection of physical parameters. The purpose is to give empirical anisotropy coefficients similar to correction coefficients according to the experimental results. This reflects the difference of physical parameters such as elastic modulus and Poisson's ratio in different directions. Although the soil has primary anisotropy, under certain conditions, if the confining pressure is large enough, the structural anisotropy can be eliminated and the soil has initial isotropy. If the unequal stress is added at this time, the soil will be in the state of anisotropic stress, and the soil will have anisotropy, which is the secondary anisotropy.

Secondary anisotropy of soils is due to the inconsistency of mechanical properties of soils in different directions caused by complex stress states. In different stress states and directions, the stress-strain law of soils varies greatly. The most obvious manifestation is the asymmetry of the stress-strain matrix. In the elastic theory, the so-called elastic mechanical parameters such as elastic modulus and Poisson's ratio will no longer have the significance of physical parameters but will change with the change of stress state, which can be regarded as a function of stress state and stress history. So far, little research has been done on stress-induced anisotropy. Some of the existing achievements are generally studied from the point of view of the influence of stress path on the parameters of commonly used models. Although some scholars have used true triaxial apparatus to test and study the three-dimensional deformation characteristics of soils in the past, they have not clearly analyzed them from the angle of anisotropy. The influence of anisotropy, especially stress-induced anisotropy, on the constitutive relationship of soil, the numerical analysis of practical geotechnical problems, and how to simulate them in the calculation have seldom been systematically studied. The preliminary study also shows that the lateral strain in the direction of small principal stress caused by loading in the direction of large principal stress is quite different from that in the direction of large principal stress caused by loading in the direction of small principal stress. The elastic theory analysis means that Poisson's ratio in the two directions is quite different. In a sense, secondary anisotropy contains the original anisotropy and has a wider significance.

2.3. Coupling of Seepage and Stress in Nonmaterial Geotechnical Materials. Fluid-solid coupling mechanics is a branch of mechanics. It is derived from the intersection of fluid

mechanics and solid mechanics. It mainly studies the influence of solid configuration on the flow field and the interaction between the changes of behavior of deformed solid under the action of the flow field. The coupling of the seepage field and stress field of immaterial geotechnical materials is a difficult problem in tunnel engineering practice. Because of the change of initial stress of surrounding rock caused by tunnel excavation, immaterial geotechnical materials occur in rock mass under load. Nonmaterial geotechnical material is the main water passage of rock mass, and its water-passing capacity is proportional to the cubic width of nonmaterial geotechnical material (cubic law), so the change of stress field will change the geometric characteristics of nonmaterial geotechnical material, such as openness, roughness, area of nonmaterial geotechnical material, and porosity. The distribution of groundwater in nonmaterial geotechnical materials is changed, and the seepage field of the rock mass is changed. Conversely, these changes will affect the distribution of the stress field of nonmaterial geotechnical materials. Therefore, the study of the coupling problem of seepage field and stress in the rock mass is beneficial to the perfection of fluid-solid coupling theory and has important engineering practice value.

This paper intends to break through the original theoretical framework of seepage stress misalignment consolidation based on effective stress principle, introduce physical quantities that can reflect seepage stress misalignment effect into the stress-strain constitutive relationship of geotechnical materials, and establish a constitutive model of soft rock which can directly reflect seepage stress misalignment effect according to the test results under simplified conditions. For the first time, the mathematical expression of the constitutive response of geotechnical materials, which can directly reflect the seepage stress coupling effect, is proposed. Permeability coefficient represents the permeability and permeability of geotechnical media. As a characteristic parameter reflecting porous media seepage and nonmaterial geotechnical material seepage, permeability coefficient is the key to the study of seepage stress combination. Previous studies have shown that the permeability coefficient is a variable, which is usually expressed as a function of stress and strain. The permeability coefficient is introduced into the existing stress-strain relationship. On the basis of the simplified experimental conditions and the assumptions in this paper, a seepage stress coincidence constitutive model is proposed as follows:

$$\sigma = f(\varepsilon, K(\varepsilon)). \tag{4}$$

The above formula is a general mathematical description of the seepage stress-strain relationship proposed in this paper. It can directly reflect the synergistic effect of seepage stress. As the key of numerical analysis and calculation, the establishment of a seepage stress coincidence constitutive model will simplify the process of coincidence calculation and improve the accuracy of the calculation. Based on the above ideas, a mathematical description of the constitutive relation of soft rock considering the factors of seepage stress conjugation is proposed by using Hooke's law and combining the existing experimental results.

$$\sigma_d = (\sigma_1 - \sigma_3) = G(\varepsilon_1) \cdot K(\varepsilon_1, k_0). \tag{5}$$

When considering the seepage stress coupling effect, the permeability coefficient is a variable, which is usually expressed as a function of stress and strain.

$$\begin{aligned} K &= f(\sigma) \\ K &= f(\varepsilon). \end{aligned} \tag{6}$$

Based on the test results and regression analysis, the relationship curve between permeability coefficient and strain is presented.

$$K(\varepsilon_1, k_0) = a \exp\left(-\frac{\varepsilon_1}{b}\right) + k_0. \tag{7}$$

In the formula, ε_1 is the strain of longitudinal axial and k_0 is the initial permeability coefficient measured for the test. a and b are the test parameters, where LT^{-1} is the dimension of a, and b is dimensionless.

Based on the experimental results, regression analysis is used to obtain the following conclusions:

$$G(\varepsilon_1) = m(\varepsilon_1 + \varepsilon_0). \tag{8}$$

The first test reflects the relationship between permeability coefficient and stress of soft rock under different strains. $\sigma_1 - \sigma_3$ is the main stress difference in the middle of the formula. ε_0 is the initial strain of the rock sample and m is the test parameter. Its dimension is FTL^{-3}. It should be pointed out that the initial strain of the rock sample exists because the axial and radial pressure is required for the end and radial sealing of the specimen in the seepage stress coincidence test. At the same time, because of the existence of axial and radial pressure during sealing, the expansion of nonmaterial geotechnical materials is limited, which results in some errors in the study of the permeability change law during the expansion process of fractured rock nonmaterial geotechnical materials.

Thus, the constitutive model of seepage stress coincidence in soft rock is derived.

$$\sigma_d = (\sigma_1 - \sigma_3) = m(\varepsilon_1 + \varepsilon_0) \cdot \left[a \exp\left(-\frac{\varepsilon_1}{b}\right) + k_0\right]. \tag{9}$$

The incremental modulus of the stress-strain relationship can be obtained by a differential equation.

$$E_t^t = am\left[1 - \frac{1}{b}(\varepsilon_1 + \varepsilon_0)\right]\exp\left(-\frac{\varepsilon_1}{b}\right) + mk_0. \tag{10}$$

In the formula, let $\varepsilon = 0$; then, the initial value of E_t^t can be expressed as

$$E_{t_0}^t = am\left[1 - \frac{\varepsilon_0}{b}\right] + mk_0. \tag{11}$$

The relationship curve between longitudinal strain ε_1 and transverse strain ε_3 adopts the following formula:

$$\varepsilon_1 = \frac{\varepsilon_3}{c + d\varepsilon_3}. \tag{12}$$

In the formula, c and d are the test parameters. Differential equations can be obtained.

$$u_1 = -\frac{\mathrm{d}\varepsilon_3}{\mathrm{d}\varepsilon_1} = \frac{c}{\left(1 - \mathrm{d}\varepsilon_1\right)^2}, \tag{13}$$

$$u_1|_{t_1=0} = c = -u_0. \tag{14}$$

In the formula, u_0 is the initial Poisson's ratio; the group, the tangent Poisson's ratio, and the initial Poisson's ratio are affected by confining pressure.

$$u_0 = f - g\,\log\left(\frac{\sigma_3}{P}\right). \tag{15}$$

In the formula, f and g are the experimental fitting parameters.

2.4. Filter Layer Controlling Seepage. Filtration and decompression of soil are the two most basic requirements of the filter layer and also the basic principle of antiseepage function of the filter layer. Only when these two basic principles are satisfied can it be ensured that the soil can be prevented from seepage failure. Filter soil is one of the main functions of the filter layer. Although there are more than thirty or forty design methods for the filter layer at present, in terms of the filter soil, including the Taisha benchmark, the following principles are followed: the particles of the protected soil are not allowed to pass through the pore of the filter layer in large quantities, leading to loss. Namely,

$$\frac{D_0}{d_k} = a_1. \tag{16}$$

In the formula, D_0 is the effective pore diameter of the filter layer, d_k is the particle size of the protected soil without seepage damage, and α_1 is the number of particles that may form an arch at the pore entrance of the filter layer to prevent other particles from entering which is also called the arch coefficient.

For seepage flow, because the filter layer is located in the lower part of the protected soil, it is necessary to lay the filter layer first and then the protective soil. During the construction process, the large particles controlling the seepage stability in the protected soil will let several particles entering the pore of the filter layer at the same time appear under the action of gravity. It is easy to form a stable arch structure consisting of three particles at the entrance of the filter layer. As shown in Figures 2 and 3(a), at this point $a_1 \le 3$, this type of filter is called type I filter. In the case of upward seepage direction, the filter layer is located at the upper part of the protected soil, and the controlled particle size in the protected soil enters into the filter layer only under the condition of a large hydraulic gradient. Therefore, most of the filters enter the filter pore in the form of a single particle successively, while the maximum particle entering the filter pore will not exceed two soil particles, especially piping soil.

Therefore, the safety value of the arching coefficient should be $a_1 \le 2$, as shown in Figure 2–3(b), which is called a type II filter.

According to the working characteristics of the above filter layer, formula (12) can be written as follows:

$$\frac{D_0}{d_k} \le 1 \sim 3. \tag{17}$$

The permeability coefficient of the filter layer must be significantly greater than that of the protected soil if the pressure is to disappear after seepage into the filter layer. According to the seepage calculation theory of double-layer medium, when seepage flows from one layer of soil to another, the hydraulic ratio of seepage in two layers of soil shows the following relationship:

$$\frac{J_1}{J_2} = \frac{K_2}{K_1}. \tag{18}$$

In the formula, k_1 and J_1 are the permeability coefficient of the filter layer and the actual hydraulic gradient it bears; k_2 and J_2 are the permeability coefficient of the protected soil and the actual hydraulic gradient it bears. The hydraulic gradient is inversely proportional to permeability coefficient in two layers of soil.

3. Experiments

3.1. Selection of Test Materials. Sedimentary rocks are one of the most widely distributed rocks in the crust. Sedimentary rock resources are widely distributed in China. Sedimentary rocks are widely distributed on the surface, accounting for about 75% of the land area. The sedimentary rock distribution area is the main site of hydrogeology and engineering geology. Laboratory tests of rocks usually have greater discreteness. When the results are analyzed, the mechanical properties of rocks can hardly be summarized or even the opposite conclusion can be drawn. However, the nonmaterial geotechnical materials in limestone have less influence on the mechanical properties of rocks. Selecting limestone to make samples can avoid the resulting error caused by some microimmaterial geotechnical materials in seepage test of nonmaterial geotechnical materials. Limestone is homogeneous in lithology, easy to be mined and processed, and has obvious characteristics under the action of groundwater and stress environment. It is suitable for rock seepage test material.

3.2. Preparation of Limestone Samples. Firstly, the selected experimental limestone blocks are cut into smaller size blocks by a cutting machine, then these blocks are made into square blocks with a height of 110 mm by a rock cutting machine, and then the blocks are put into the rock coring machine. Standard test rock samples with a height of 110 mm and diameter of 40 mm were prepared by water drilling method (using tap pipe to add water and working together with core drill bit). Then, the samples were screened and classified, and the rock samples with damaged side, too large gap at both ends, sandy soil, and obvious cracks in

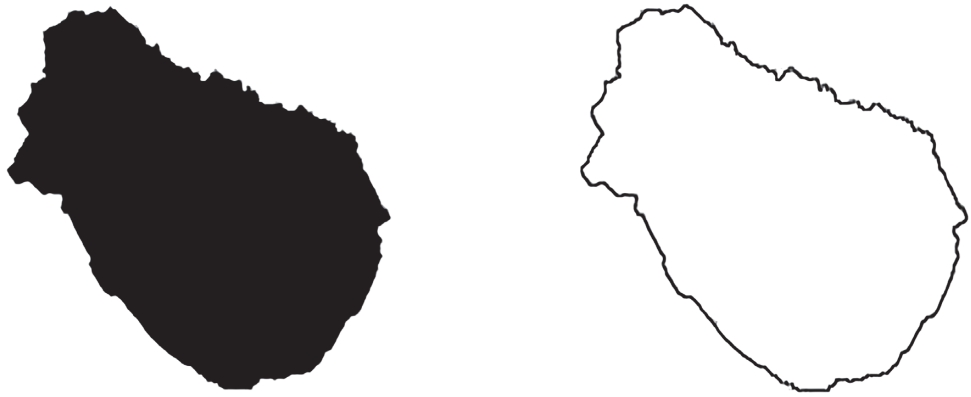

Figure 2: Edge detection of stone.

(a) (b)

Figure 3: Types and working principles of the filter layer. (a) I type reverse filtration. (b) II type reverse filtration.

material were removed and grouped again to reduce the influence of individual differences on the seepage test.

In the preparation of rock samples, because of uneven ground, the vibration of mechanical equipment in the process of processing, cutter carton, the too fast loading speed of coring machine, and other human factors result in the faults of the uneven end face and lack of standard rock samples. For these shortcomings, the rock grinder is used in the preparation of rock samples. Through two diamond grinding wheels, the equipment grinds two parallel end faces to grind the rock samples at the same time. In addition, the grinding tool stone is used to grind the rock samples equally and especially to ensure that the end faces of the rock samples are smooth so that the flatness of the end faces can reach the standard requirements of +0.05 mm. In addition, when grinding the end face, this test uses a simple device to ensure that the verticality of the rock sample does not exceed 0.25 degrees and grinds the side face of the rock sample with coarse, fine gauze, and polishing machine to ensure that the absolute value of the diameter difference between the two end faces of the rock sample is less than 0.3 mm, so that the rock sample meets the requirements of the code.

3.3. Software for Picture Processing of Experimental Rock and Soil. Hardware environment: computer Dell, CPU i7, GPU GT630M

Software environment: flagship version of operating system win10 64 bit, MATLAB

4. Discussion

For the laboratory test of one-dimensional small specimens in this paper, the axial direction of the specimens, i.e., the direction of loading, is assumed to be the direction, and the formula can be expressed as follows:

$$\sigma_{dx} = m\left(\varepsilon_x + \varepsilon_{x0}\right) \cdot \left[a \exp\left(-\frac{\varepsilon_x}{b}\right) + k_{x0}\right]. \tag{19}$$

In the formula, k_{x0} is the initial axial permeability coefficient and ε_{x0} is the initial axial strain of rock samples obtained. The incremental stress-strain relationship is as follows:

$$\mathrm{d}\sigma_x = \left[ma \exp\left(-\frac{\varepsilon_x}{b}\right) + mk_{x0} - m\left(\varepsilon_x + \varepsilon_{x0}\right)\frac{\varepsilon_x}{b} a \exp\left(-\frac{\varepsilon_x}{b}\right)\right]\mathrm{d}\varepsilon_x. \tag{20}$$

The modulus of the stress-strain relationship is

$$D = ma\ \exp\left(-\frac{\varepsilon_x}{b}\right) + mk_{x0} - m\left(\varepsilon_x + \varepsilon_{x0}\right)\frac{\varepsilon_x}{b}a\ \exp\left(-\frac{\varepsilon_x}{b}\right). \quad (21)$$

Based on several theories, the stress-permeability coefficient-strain test data of soft rock are 100# and 158#; based on the analysis of the test results, the stress-strain curves of rock samples can be obtained by seepage above mountains and stress-strain constitutive relations. The values of test parameters in the texture relationship of each rock sample obtained from the analysis of the test results of each rock sample are shown in Table 1.

The stress-strain relationship calculation curve is shown in the smooth curve as shown in Figures 1 and 2.

The comparison of Figures 4 and 5 shows that the strength values of the same rock samples in different directions are different. The strength values of rock samples parallel to the bedding direction are lower, while the strength values of rock samples perpendicular to the bedding direction are higher, which is reflected in the stress-strain relationship; that is, the value of parameter m is larger. It can be seen from the comparison that the relationship between permeability coefficient and strain of the two rock samples under compression is different, which is reflected in the difference of a value in the constitutive equation. It can be seen from the comparison that the nonlinear relationship between stress and strain of the two rock samples under compression is different, which is reflected in the difference of B value in the constitutive equation. In Figures 4 and 5, it can be seen from the agreement between the experimental results and the calculated results that the stress-strain relationship proposed in this paper, which can take into account the influence of seepage, can better describe the stress-strain characteristics of the elastic stage and the nonlinear strengthening stage of soft rock with seepage.

The preservation of some of the edge details of the image can make the fractal dimension more accurate, and some noise suppression will also reduce the difficulty of subsequent processing. Therefore, the smoothing method here must achieve a good balance between eliminating noise and enhancing or protecting image features. In suppressing noise, the traditional filtering method embodies the trade-off between image signal-to-noise ratio and spatial resolution. Mean filtering smooths the image to eliminate evenly distributed noise and Gaussian noise in the image at the expense of blurring the original image. Figures 6 and 7 show the digital image processing.

The normal deformation curves of nonmaterial geotechnical materials and blocks can be obtained by experiments. As shown in Figure 8, the normal deformation values of nonmaterial geotechnical materials and blocks are shown in the figure. For the normal displacement of rock blocks in nonmaterial geotechnical materials, the weighted values of deformation of coarse sandstone blocks and fine sandstone blocks without structural planes can be obtained.

The curves of nonmaterial geotechnical materials can be obtained. By analyzing and studying Figure 6, the normal stiffness coefficient of cracks $\sigma_n = 10$ MPa is taken as the

Table 1: Test parameter values in the texture relationship of rock samples.

Specimen/parameter	a	b	m	K_0	ε_0
100#	-1.28×10^{-8}	0.062	2.14×10^{12}	1.96×10^{-12}	0.5
158#	5.1×10^{-16}	0.4	0.91×10^{17}	2.3×10^{-17}	−0.93

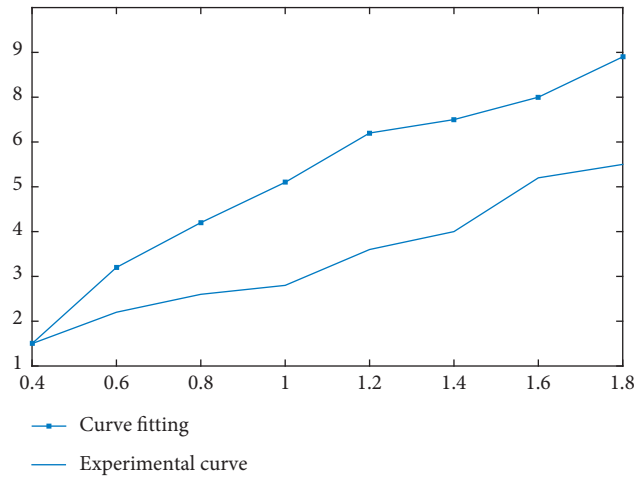

Figure 4: Comparisons of stress-strain relationship test results and juice calculation curves for 100#.

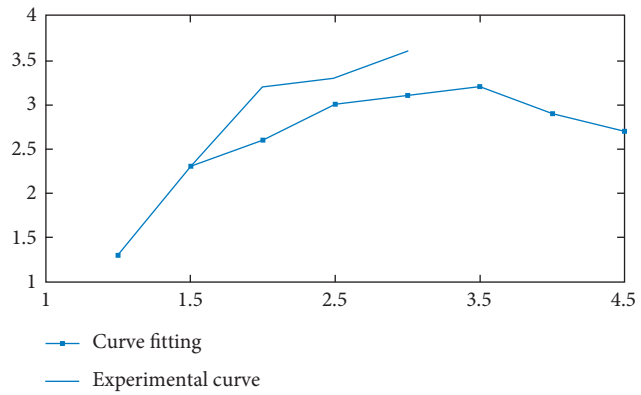

Figure 5: The stress-strain relationship test results of 158# and the fitting curve comparison chart.

unified stiffness coefficient of nonmaterial geotechnical material structural planes under different confining pressures. The normal stiffness coefficients of single-fissure coarse sandstone, single-fissure fine sandstone, and nonmaterial rock and soil materials are 1.793, respectively, by solving the slope of a point on the curve $o_n - \Delta d_f$.

Under different confining pressures, the failure mode of coarse sandstone and fine sandstone is mainly the shear failure of the oblique section after unloading. Specific steps are as follows: (a) measure the diameter and height of the specimen accurately, as shown in Table 2; (b) place the standard rock specimen between the upper and lower bases with gaskets in the test, seal with tape, and then add a heat shrinkage tube to ensure uniform and close contact between

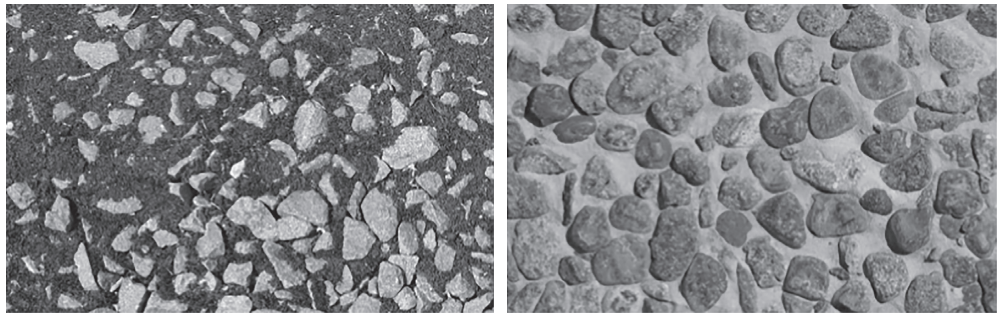

Figure 6: Performs over-limit neighborhood averaging (3 × 3) processing.

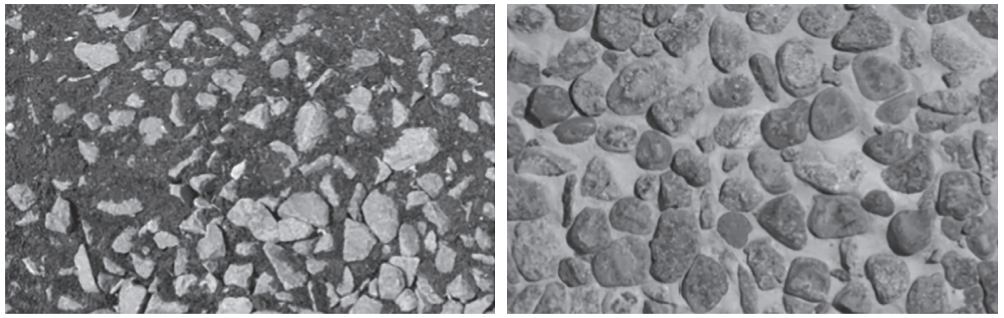

Figure 7: Performs over-limit neighborhood averaging (5 × 5) processing.

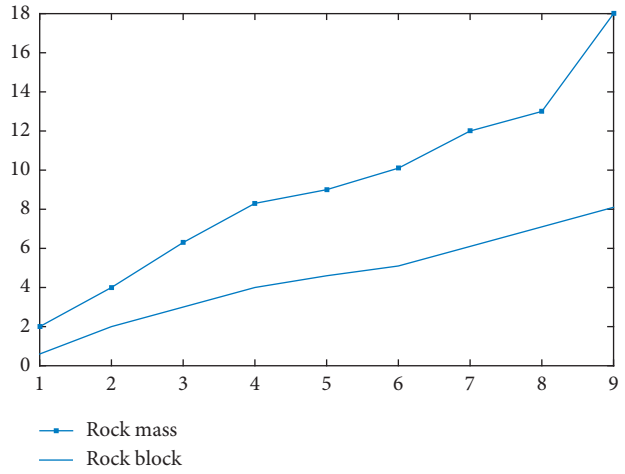

Figure 8: Weighted value curve.

Table 2: Dimensions and confining pressures of specimens.

Specimen number	Diameter (mm)	Height (mm)	Confining pressure (MPa)
01	46	97	0
02	47	96	2
03	48	95	4
04	49	96	6

the heat shrinkage tube and the specimen; (c) install an extensometer and a hoop device on the specimen; (d) place the installed pattern on the test machine; (e) apply confining pressure first and then axial pressure through the computer system of the test machine, and reasonably control loading path, loading rate, and data sampling interval in advance.

Table 2 shows that the stress-strain curves of standard rock specimens vary basically under different confining pressures, but there are some differences in peak strength, residual strength, and yield stress with different confining pressures.

5. Conclusions

The constitutive theory of nonmaterial geotechnical materials is the basis of modern soil mechanics. When using advanced numerical methods to analyze geotechnical engineering problems, the correct establishment and rational application of the geotechnical media constitutive model is often one of the key technologies to improve the accuracy of calculation, which is of great significance. In the study of permeability and hydraulic hazard of nonmaterial geotechnical materials, one of the most critical problems is the determination of a constitutive model of geotechnical materials. Due to the limitation of experimental means and theoretical development stage, the constitutive model of seepage stress coincidence has not yet been systematically reported. In this paper, based on the analysis of anisotropic seepage stress coincidence in geotechnical engineering, the constitutive model of anisotropic seepage stress coincidence in soft rock material is established on the basis of the analysis of the modeling theory and research status of the constitutive model of geotechnical material and the results of the seepage stress coincidence test in soft rock. The main achievements of this paper are as follows:

(a) In this study, the calculation models and theoretical formulas of permeability coefficients of nonmaterial

geotechnical materials with different lithologies on both sides of cracks are derived, which improves the accuracy of the calculation of permeability coefficients of heterogeneous nonmaterial geotechnical materials. The proposed formula complements the short slabs in this field and provides a more safe and reliable calculation method for geotechnical engineering construction

(b) The permeability coefficient of nonmaterial geotechnical materials decreases with the increase of confining pressure in a certain range. When the net confining pressure is 14 MPa, the permeability coefficient of nonmaterial geotechnical materials begins to stabilize, which indicates that the influence of confining pressure on the permeability of rock mass is limited to a certain range

(c) Lithology on both sides of the fracture surface of immaterial geotechnical materials has a significant influence on the fracture permeability coefficient. Under the same fissure water pressure and confining pressure, the permeability coefficient of single-fissure coarse sandstone is the largest, the permeability coefficient of the single-fissure heterogeneous rock mass is the second, and the permeability coefficient of single-fissure fine sandstone is the smallest

Data Availability

No data were used to support this study.

Conflicts of Interest

The authors declare that they have no conflicts of interest.

Acknowledgments

This work was supported by General Programs of the National Natural Science Foundation of China (Grant no. 51774184).

References

[1] L.-D. Yi, H.-B. Lv, T. Ye, and Y.-P. Zhang, "Quantification of the transparency of the transparent soil in geotechnical modeling," *Advances in Civil Engineering*, vol. 2018, Article ID 2915924, 8 pages, 2018.

[2] V. B. Patil, A. S. Bhanage, and R. S. Patil, "Analysis and optimization of process parameters of abrasive flow machining process for super finishing of non-ferrous material nozzle," *Applied Mechanics and Materials*, vol. 612, pp. 97–104, 2014.

[3] M. K. Paesold, A. Karrech, T. Dodwell et al., "Non-linear thermo-mechanics of folding in geomaterials," in *Proceedings of the International Association for Mathematical Geosciences*, pp. 753–756, New Delhi, India, October 2014.

[4] M. Jiang, F. Zhu, F. Liu et al., "A bond contact model for methane hydrate-bearing sediments with interparticle cementation," *International Journal for Numerical & Analytical Methods in Geomechanics*, vol. 38, no. 17, pp. 1823–1854, 2015.

[5] C. Jiang, C. Wang, and L. Kong, "Estimation of the surface roughness of K9 optical glass in precision grinding using the brittle material removal fraction based on an improved image processing algorithm," *Insight—Non-destructive Testing and Condition Monitoring*, vol. 58, no. 5, pp. 240–245, 2016.

[6] Z. Li, H. Liu, Z. Dun, L. Ren, and J. Fang, "Grouting effect on rock fracture using shear and seepage assessment," *Construction and Building Materials*, vol. 242, p. 118131, 2020.

[7] S. M. Kopinski, "Use of computer simulations and levels of integration and commitment for nontraditional commuter students," Doctoral dissertation, Walden University, Minneapolis, MN, USA, 2014.

[8] J. F. Shao and J. W. Rudnicki, "A microcrack-based continuous damage model for brittle geomaterials," *Key Engineering Materials*, vol. 177-180, no. 10, pp. 103–108, 2016.

[9] J. L. Aragones, M. Rovere, C. Vega, and P. Gallo, "Computer simulation study of the structure of LiCl aqueous solutions: test of non-standard mixing rules in the ion interaction," *The Journal of Physical Chemistry B*, vol. 118, no. 28, pp. 7680–7691, 2014.

[10] P. Hajko and J. Tejchman, "Modelling of shear localization during granular flow within non-local hypoplasticity using material point method," in *Springer Series in Geomechanics and Geoengineering: International Workshop on Bifurcation and Degradation in Geomaterials*, pp. 593–598, Springer, Cham, Switzerland, 2017.

[11] I. S. A. Sulem, "Chemically induced compaction bands: triggering conditions and band thickness," *Journal of Geophysical Research Solid Earth*, vol. 119, no. 2, pp. 880–899, 2014.

[12] C. Peng, W. Wu, H.-s. Yu, and C. Wang, "A SPH approach for large deformation analysis with hypoplastic constitutive model," *Acta Geotechnica*, vol. 10, no. 6, pp. 703–717, 2015.

[13] K. D. Kanagawa, T. Muto, H. Tanaka et al., "Mass constraint for a planet in a protoplanetary disk from the gap width," *Publications-Astronomical Society of Japan*, vol. 68, no. 3, p. 37, 2016.

[14] A. K. M. F. Rahman, J. D. Lynch, and E. A. Peña, "Nonparametric Bayes estimation of gap-time distribution with recurrent event data," *Journal of Nonparametric Statistics*, vol. 26, no. 3, pp. 575–598, 2014.

[15] S. Deng, L. Lu, H. Liu et al., "Pore-fractural network model for compacted geomaterials and simulation of shale gas seepage," *Chinese Journal of Underground Space & Engineering*, vol. 11, no. 3, pp. 76–79, 2015.

[16] W. Sun, Q. Chen, and J. T. Ostien, "Modeling the hydro-mechanical responses of strip and circular punch loadings on water-saturated collapsible geomaterials," *Acta Geotechnica*, vol. 9, no. 5, pp. 903–934, 2014.

[17] Q. Liu, Y. Cheng, H. Zhou, P. Guo, F. An, and H. Chen, "A mathematical model of coupled gas flow and coal deformation with gas diffusion and Klinkenberg effects," *Rock Mechanics and Rock Engineering*, vol. 48, no. 3, pp. 1163–1180, 2015.

[18] X. Zhang, M. Mavroulidou, and M. J. Gunn, "Mechanical properties and behaviour of a partially saturated lime-treated, high plasticity clay," *Engineering Geology*, vol. 193, pp. 320–336, 2015.

[19] I. Miličević, N. Štirmer, and I. B. Pečur, "Residual mechanical properties of concrete made with crushed clay bricks and roof tiles aggregate after exposure to high temperatures," *Materials*, vol. 9, no. 4, p. 295, 2016.

[20] B. Chen, J. Li, X. Li et al., "Achieving high thermal and mechanical properties of epoxy nanocomposites via incorporation of dopamine interfaced clay," *Polymer Composites*, vol. 39, no. S4, pp. E2407–E2414, 2017.

[21] F. Liu, J. S. Chen, and K. W. Li, "Experimental analysis of mechanical properties of high organic soft clay at different depths," *Advanced Materials Research*, vol. 1056, pp. 52–57, 2014.

[22] H. Z. D. H. Zhen Li, "Yield criterion for rocklike geomaterials based on strain energy and CMP model," *International Journal of Geomechanics*, vol. 20, no. 3, Article ID 04020013, 2020.

[23] H. U. Tianfei, J. Liu, J. Fang et al., "Experimental study on the effect of cyclic freezing-thawing on mechanical properties of silty clay under different cooling temperatures," *Chinese Journal of Rock Mechanics & Engineering*, vol. 33, no. 7, pp. 1496–1502, 2017.

[24] Y. Li, S. Xu, H. Liu, E. Ma, and L. Wang, "Displacement and stress characteristics of tunnel foundation in collapsible loess ground reinforced by jet grouting columns," *Advances in Civil Engineering*, vol. 2018, Article ID 2352174, 16 pages, 2018.

[25] C. Sadik, I.-E. El Amrani, and A. Albizane, "Recent advances in silica-alumina refractory: a review," *Journal of Asian Ceramic Societies*, vol. 2, no. 2, pp. 83–96, 2014.

[26] A. Mahamedi and M. Khemissa, "Stabilization of an expansive overconsolidated clay using hydraulic binders," *HBRC Journal*, vol. 11, no. 1, pp. 82–90, 2015.

[27] M. Pastor, T. Blanc, B. Haddad et al., "Depth averaged models for fast landslide propagation: mathematical, rheological and numerical aspects," *Archives of Computational Methods in Engineering*, vol. 22, no. 1, pp. 67–104, 2015.

[28] T. V. Duong, Y.-J. Cui, A. M. Tang et al., "Effects of water and fines contents on the resilient modulus of the interlayer soil of railway substructure," *Acta Geotechnica*, vol. 11, no. 1, pp. 51–59, 2016.

[29] J. Choo and R. I. Borja, "Stabilized mixed finite elements for deformable porous media with double porosity," *Computer Methods in Applied Mechanics and Engineering*, vol. 293, pp. 131–154, 2015.

[30] E. S. S. A. Seif, "Geotechnical approach to evaluate natural fine aggregates concrete strength, Sohag, Governorate, Upper Egypt," *Arabian Journal of Geosciences*, vol. 8, no. 9, pp. 1–11, 2014.

[31] R. Asadi and B. Ataie-Ashtiani, "A comparison of finite volume formulations and coupling strategies for two-phase flow in deforming porous media," *Computers and Geotechnics*, vol. 67, pp. 17–32, 2015.

[32] B. Mao, "Application of the vertically-mixed runoff model to the calculation of the rainfall threshold of flash floods in ungauged basins," *Journal of Basic Science and Engineering*, vol. 24, no. 4, pp. 720–730, 2016.

[33] J. V. Ruette, P. Lehmann, and D. Or, "Linking rainfall-induced landslides with predictions of debris flow runout distances," *Landslides*, vol. 13, no. 5, pp. 1–11, 2015.

[34] K. K. Chandra, A. K. Bhardwaj, K. K. Chandra et al., "Incidence of forest fire in India and its effect on terrestrial ecosystem dynamics, nutrient and microbial status of soil," *International Journal of Agriculture & Forestry*, vol. 5, no. 2, pp. 69–78, 2015.

[35] J. Abd Rahman, "*Relationship between decomposition level and induced solidification of peat based on laboratory investigation*," M.S. thesis, University Tun Hussein Onn Malaysia, Parit Raja, Malaysia, 2015.

[36] S. A. Hamoudi, B. Hamdi, and J. Brendlé, "Removal of ions Pb^{2+} and Cd^{2+} from aqueous solution by containment geomaterials," *Exergetic, Energetic and Environmental Dimensions*, pp. 1029–1043, 2018.

[37] M. J. Alipour and A. Lashkari, "Prediction of sand instability under constant shear drained paths," in *Proceedings of the International Workshop on Bifurcation and Degradation in Geomaterials*, pp. 105–110, Limassol, Cyprus, May 2017.

[38] A. Eslami, M. Ahmadnezhad, A. E. Kenarsari et al., "Experimental study on stiffness properties of non-engineered clay and granular fills," *Arabian Journal of Geosciences*, vol. 8, no. 5, pp. 1–11, 2015.

[39] S. Ji, S. Sun, and Y. Yan, "Discrete element modeling of rock materials with dilated polyhedral elements," *Procedia Engineering*, vol. 102, pp. 1793–1802, 2015.

[40] P. Shan and X. Lai, "Influence of CT scanning parameters on rock and soil images," *Journal of Visual Communication and Image Representation*, vol. 58, no. 1, pp. 642–650, 2019.

[41] S. Wan, Y. Xia, L. Qi, Y. H. Yang, and M. Atiquzzaman, "Automated colorization of a grayscale image with seed points propagation," *IEEE Transactions on Multimedia*, vol. 22, no. 7, pp. 1756–1768, 2020.

[42] P. Shan and X. Lai, "Mesoscopic structure PFC~2D model of soil rock mixture based on digital image," *Journal of Visual Communication and Image Representation*, vol. 58, pp. 407–415, 2019.

[43] Nhat-Duc Hoang and Q.-L. Nguyen, "Metaheuristic optimized edge detection for recognition of concrete wall cracks: a comparative study on the performances of roberts, prewitt, canny, and sobel algorithms," *Advances in Civil Engineering*, vol. 2018, Article ID 7163580, 16 pages, 2018.

[44] M. Elhoseny and K. Shankar, "Optimal bilateral filter and convolutional neural network based denoising method of medical image measurements," *Measurement*, vol. 143, pp. 125–135, 2019.